Open Access

A 1-D Heterodyne Lens-Free Optical Phased Array Camera With Reference Phase Shifting

Behrooz Abiri, *Student Member, IEEE*
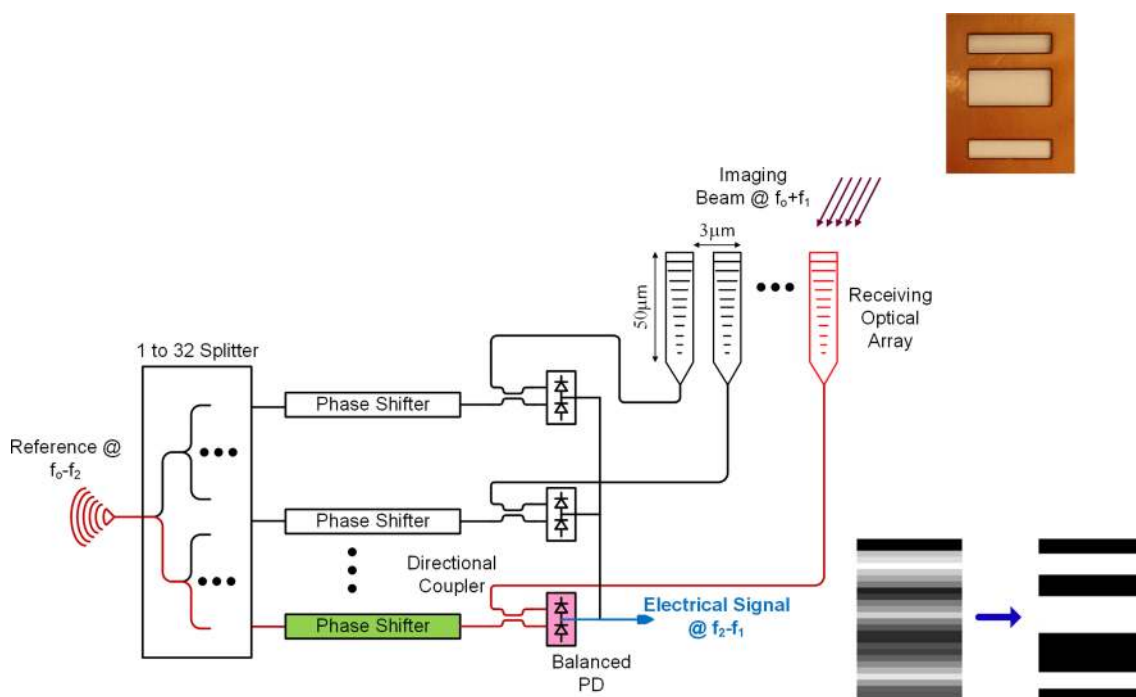**Reza Fatemi**, *Student Member, IEEE*
Ali Hajimiri, *Fellow, IEEE*

photonics SOCIETY

IEEE

A 1-D Heterodyne Lens-Free Optical Phased Array Camera With Reference Phase Shifting

Behrooz Abiri, *Student Member, IEEE*,
Reza Fatemi ⓘ, *Student Member, IEEE*,
and Ali Hajimiri ⓘ, *Fellow, IEEE*

California Institute of Technology, Pasadena, CA 91125 USA

Abstract: This paper presents the first integrated silicon photonics optical phased array (OPA) receiver with imaging capabilities. A 32-element one-dimensional (1-D) OPA with an overall aperture size of 96×50 μm^2 is used to generate an electrically steerable "gazing beam." The OPA receiver elements couple the incident light to on-chip waveguides that is processed as a phased array receiver. To minimize signal loss and enhance sensitivity, a heterodyne architecture with phase shifters in the local reference path is utilized. The OPA receiver can provide fully programmable angular selectivity with a grating-lobe-free field-of-view of 30° and a gazing beamwidth of 0.74°.

Index Terms: Silicon nanophotonics, integrated photonic systems, imaging systems, nano-antennas, applications.

1. Introduction

Silicon photonics fabrication processes have enabled integration of many optical elements on a single chip. On-chip high performance components such as modulators [1]–[3], grating couplers [4], [5], lasers [6], [7], and photodiodes [8], [9] in close proximity enable novel systems and architectures not practical in bench-top settings. Furthermore, the hybrid photonic-electronic integrated circuits [10]–[12] with the eventual co-integration enables new approaches not practical in either of the platforms by themselves. OPA transmitters are an example of such systems that have attracted much interest recently [13]–[19]. An OPA transmitter includes an array of grating couplers that radiates light out of the chip. By controlling the phase of the light feeding each radiating element, a beam can be formed and steered to send the light to a desired direction analogous to microwave phase array transmitters [20], [21]. Since electromagnetic wave propagation is reciprocal, in principle, a similar array structure can detect and determine the light intensity arriving from a particular angle, thereby forming what can be called a gazing beam, when operating as a phased array receiver. In radio frequency systems, phased array receivers have been investigated and implemented in the past [22] based on this concept. An optical phased array receiver with beamforming and steering
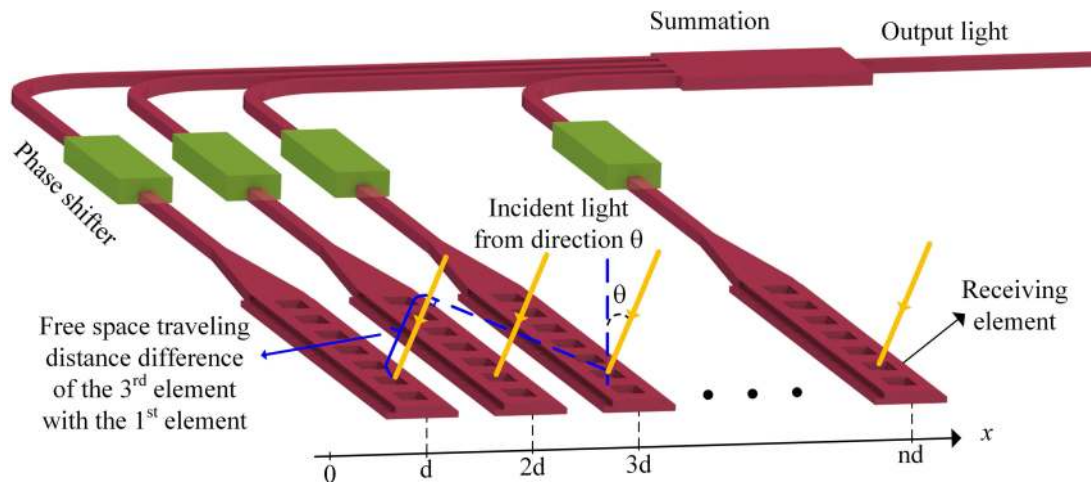
Fig. 1. Conceptual schematic of a 1D direct conversion optical phased array receiver.

capabilities can serve many purposes, including functioning as a lens-free camera [23], compact LiDAR [24], [25], active sensor, etc.

The trade-offs in an OPA receiver are qualitatively and quantitatively different from those in an OPA transmitter as the signal-to-noise levels are substantially different in an OPA receiver. There are challenges in designing an OPA transmitter, such as achieving high efficiency and controlling stray light which is the portion of input light that does not couple to the chip [15]–[17]. On the other hand, the main challenge in a receiver system is the very weak signal picked up by each element. Therefore, using an OPA transmitter architecture as a receiver (as the reciprocity principle suggests) [26] would not be very effective. In such a direct conversion phased array receiver that uses a transmitter architecture, the signal will be further attenuated by the phase shifters in the signal path that degrades its performance. Thus, the OPA receiver must adopt a different architecture to handle and process the received light accordingly [27], [28].

This paper presents the first one-dimensional OPA receiver with heterodyne detection [27] that can selectively collect light from a desired direction in the presence of noise and interference. A heterodyne architecture eliminates the signal loss in the phase shifters and can instead provide conversion gain to enhance the OPA receiver's sensitivity. Scanning the field-of-view by steering the gazing beam and forming an image of the target in front of the chip by assembling the signal associated with different bearings, can effectively turn the OPA receiver into a lens-free camera.

In the following sections, we start with a brief explanation of the fundamentals of the phased array receiver and its use as an imager. Next, we will discuss the details of heterodyne detection scheme and the design of the presented OPA receiver. Finally, the measurement setup and experimental results are presented.

2. Phased Array Receiver

Many of the basic properties of the OPA receiver can be more easily understood in the conceptual schematic of the direct conversion (an opposed to heterodyne) OPA receiver shown in Fig. 1 where a uniform array of receiving elements forms the aperture. As Fig. 1 shows, in a uniform array, elements are placed at a spacing of d. A plane wave impinging at an angle θ arrives at different elements with different time delays. With the first element on the left at $x = d$ and the kth element at $x = kd$, the path difference that light impinging at angle θ should travel to reach the first element compared to the kth element is $kd \sin(\theta)$. Therefore, it arrives at the kth element earlier than the first
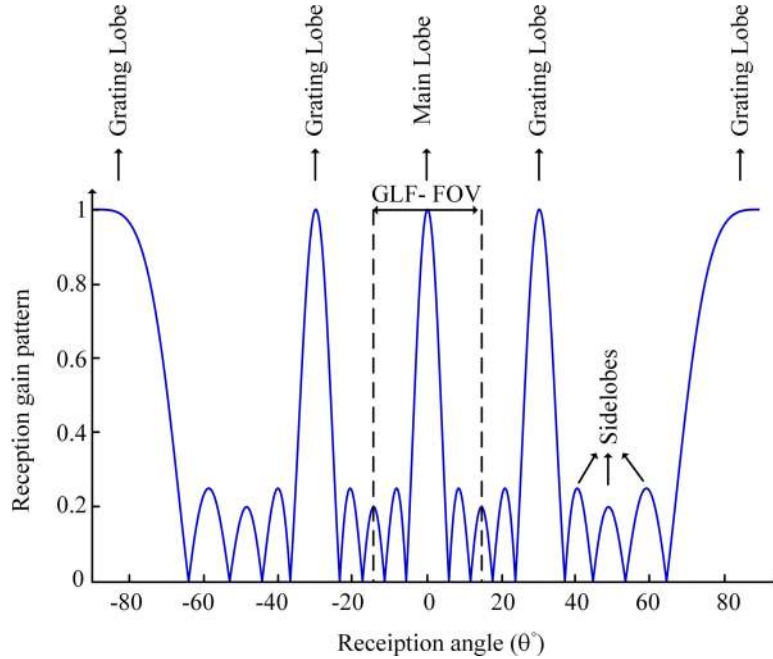
Fig. 2. Array pattern for a 5-element array with element spacing of 2λ and omni-directional elements.

element by

$$t_k = \frac{kd\sin(\theta)}{c}, \qquad (1)$$

where c is the speed of light. This time difference corresponds to a phase difference of

$$\phi_k = \frac{2\pi kd\sin(\theta)}{\lambda} \qquad (2)$$

where λ is the wavelength of the incident light. Therefore, with a plane wave impinging at an angle θ, the electric field received by the kth element is

$$E_k(t) = E_0 e^{j(\omega_0 t + \phi_k)} \qquad (3)$$

In a direct-conversion phased array receiver tuned to receive light from angle θ_0, the time of arrival difference is compensated by applying the phase shift

$$\psi_k = \frac{2\pi kd\sin(\theta_0)}{\lambda} \qquad (4)$$

to the coherent light received from the kth element. Therefore, all the signals associated with the wave front impinging at θ_0 will be in-phase after the phase shifts are applied. Summing the signals in this setting results in a constructive interference for the light coming from direction $\theta = \theta_0$. This effectively steers the receiver gazing beam to the angle θ_0. Assuming an omni-directional receiving element pattern, the resulting output signal after the summation is

$$E(t) = \sum_{k=1}^{n} E_k(t) e^{-i\psi_k} = E_0 \sum_{k=1}^{n} e^{j(\omega_0 t + \phi_k - \psi_k)} = E_0 e^{j\omega_0 t} \sum_{k=1}^{n} e^{\frac{2\pi ikd\left(\sin(\theta) - \sin(\theta_0)\right)}{\lambda}} \qquad (5)$$

where n is the number of the array elements. A detector, such as a photodiode, can be used to convert the output optical signal, $E(t)$, to an electrical current.

Fig. 2 shows the normalized reception gain, *i.e.*, the magnitude of $E(t)$, for a phased array with 5 elements and element spacing $d = 2\lambda$ when ψ_ks are adjusted for $\theta_0 = 0$. Since light arriving from

angle $\theta = 0$ sums up constructively, the phased array has the maximum gain at $\theta = 0$. The lobe at θ_0 in Fig. 2 is called the main lobe. In a phased array receiver with element spacing $d > \lambda/2$ ($d = 2\lambda$ for Fig. 2), there exist other angles that signals of all the elements happen to be in phase at the summation, often called grating lobes. The angular spacing between the main lobe and a neighboring grating lobe defines the grating-lobe-free field-of-view (GLF-FOV) of the phased array, which is a function of the element spacing. The field-of-view for the example array of Fig. 2 is 30°. Other than the grating lobes, the array pattern might have minor lobes, called side lobes, appearing at angles that the phase shifted signals sum up partially constructive.

The main lobe defines the gazing beam of the OPA receiver, which is the desired direction of receiving the incident light on the chip. To receive light from a different θ_0, phase shifts should be adjusted using equation (4). Through the use of a tunable phase shifter per element to adjust ψ_k, it is possible to steer the pattern (and thereby the main lobe) to receive signals from different directions. The OPA receiver can form various gazing beams at different angles by using different phase settings. An image can be formed by scanning this gazing beam and measuring the signal received from all the directions.

The individual receiving elements also have a certain reception pattern that indicates how strong the wave coming from each angle couples into the waveguide on the chip. Grating coupler pattern depends on its geometry, constituting material, and the wavelength it is working at. The overall reception of a phased array system is the product of the receiving element pattern and the array pattern [20]. In practice, the grating lobes are often attenuated by the pattern of the individual elements, and are significantly less important. In an optimized design, the pattern of the individual receiving elements can be matched to the GLF-FOV to maximize the suppression of the spurious signal picked up from the grating lobes. Grating lobes that are not suppressed enough by the individual element pattern can also be easily filtered spatially if more grating lobe rejection is required.

3. OPA Receiver Design

3.1 Heterodyne Detection

The simple conceptual explanation of the phased array receiver in the previous section does not naturally lend itself to a practical implementation. One of the main issues is the very low strength of the received signals and the system's sensitivity to the shot noise of the photodiodes (used for converting optical signals to electrical signals) as well as the thermal noise of the electrical amplifiers collecting the photodiode signals. Moreover, stray light that is not processed by the phased array system is picked up by the photodiodes directly and produces unwanted output.

To overcome these issues, we propose a heterodyne OPA receiver architecture. In heterodyne mixing [29], two signals with different frequencies are mixed with each other and the desired mixed component is the beat tone of the two frequencies. In this approach, the light impinging on the phased array receiving elements

$$E_i(t) = a \cos[2\pi(f_0 + f_i)t + \phi_i] \tag{6}$$

has the optical frequency $f_0 + f_i$. A strong reference light with frequency $f_0 - f_r$ is the second signal in mixing, $E_{ref}(t)$, where

$$E_{ref}(t) = A \cos[2\pi(f_0 - f_r)t + \phi_r] \tag{7}$$

The mixed product of the two signals is $E_i(t)E_{ref}(t)$. The nonlinear nature of the photodiode is used to perform multiplication of the two signals. Adding the two signals and feeding the sum to a photodiode yields the low frequency component of the product, $I(t)$, which includes DC terms and a component at frequency $(f_0 + f_i) - (f_0 - f_r)$ (the beat tone), i.e.,

$$I(t) = R \left(A^2 + a^2 + 2A\,a \cos\left[2\pi(f_i + f_r)t + \phi_i - \phi_r\right]\right) \tag{8}$$
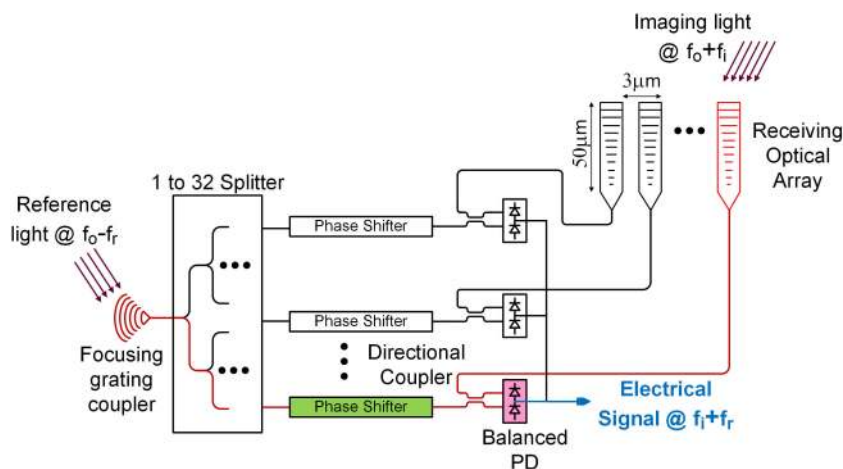
Fig. 3. The schematic of the designed heterodyne OPA receiver. Colored path shows the processing of a single element.

where R is the responsivity of the photodiode. Equation (8) shows that the amplitude of the strong reference light, A, appears as gain for the detected signal. Amplifying the incident signal before detection in this scheme improves the OPA receiver's sensitivity. In addition, the output signal of the photodiode has a different RF modulation frequency from the incident and reference lights. Therefore, it can be easily differentiated from the stray light in the post processing in the electrical domain.

While conceptually phase shifting the impinging signal may sound straightforward, the received signal generally can be very small, and therefore the signal losses due to the phase shifters can be detrimental. To overcome these challenges, we perform the phase shift in the reference path of the heterodyne receiver in an LO-phase shifting architecture. This reference phase shifting architecture has been used in RF integrated circuits in the past [22] and can be used to great effect in optical phased arrays.

3.2 System Design

Fig. 3 shows the architecture of the designed heterodyne OPA receiver, where a 1,550 nm laser is used for illumination and imaging. Thirty-two receiving elements are used as array elements with element spacing of 3 μm, which results in a theoretical 3 dB beamwidth of 0.82° and GLF-FOV of 31.1°.[1] Since the total receiver pattern is the product of the array pattern and grating coupler pattern, the beamwidth is further narrowed to 0.68°. The receiving elements are grating couplers, which are designed to efficiently couple the light impinging on their surface into the propagating mode of the dielectric waveguide connected to them. Each grating coupler is a 50 μm by 2 μm silicon slab that is 220 nm thick, along with two 0.5 μm wide, 60 nm etched slabs on the sides, as shown in Fig. 4(a). The gratings are achieved via periodic slots that are etched 60 nm into the silicon slab. The grating period is 560 nm with a 60% duty cycle. A tapered mode converter, 8 μm in length, couples the received light from the 2 μm wide slab into a dielectric waveguide with 0.5 μm width. Fig. 4 shows the grating coupler and its far-field pattern. The length of the grating coupler is along the x-axis and the width is along the y-axis. Since the width is short compared to the wavelength, 1,550 nm, the pattern is wide along the y-axis. The long dimension, 50 μm, yields a narrow pattern along the x-axis. Grating couplers are placed in a 1D array along the y-axis. The overall pattern of the phased array is the product of the grating coupler pattern and the array pattern. This results in

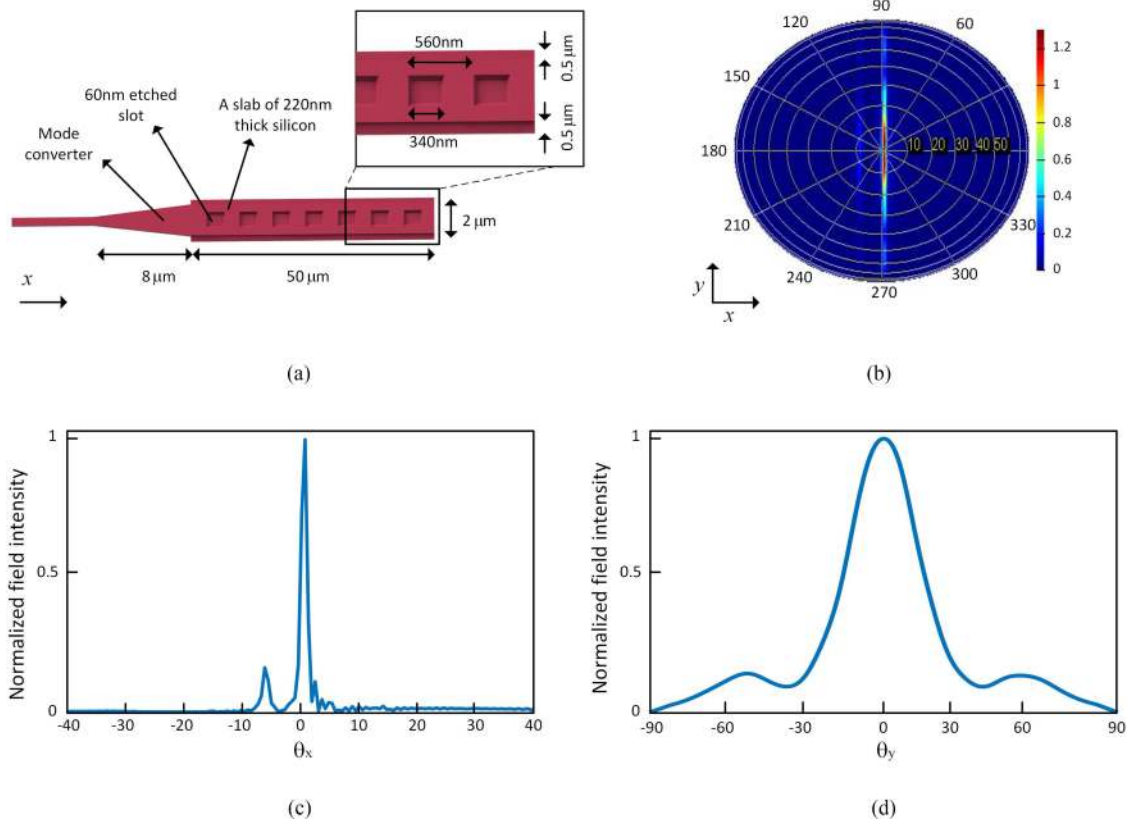[1]As a point of reference this corresponds to a lens with 50 mm focal length on a DSLR of 1.5 crop-factor.

Fig. 4. (a) Simplified illustration of the 1D receiving element. (b) Far-field reception pattern of the receiving element on a hemisphere. (c) Far-filed pattern of the receiving element at $\theta_y = 0$. (d) Far-filed pattern of the receiving element at $\theta_x = 1°$.

an overall pattern that is narrow along both axes and it is electronically steerable along the y-axis by adjusting the phase shifts applied to each element.

Directional couplers with a coupling ratio of 50% are used to combine the received light and the reference light (Fig. 3), as required for heterodyne mixing. Each directional coupler consists of two dielectric waveguides 17.7 μm in length and 0.2 μm apart. The small gap between the two waveguides results in evanescent coupling such that 50% of the light in one waveguide couples to the other waveguide after 17.7 μm of propagation. Optical signal captured by each receiving element is routed to the input port of a directional coupler. Dielectric single mode channel waveguides [13], 220 nm by 500 nm in size, are used to route optical signals on the chip. The other input port of the directional coupler is fed with a reference signal. As a result, 50% of each input port transfers to the coupled port of the directional coupler and the two output ports carry the sum of half of each input signal. Moreover, due to the 90° coupling phase shift inherent to the directional coupler, the beat tone embedded in the two output signals are 180° out-of-phase which yields a differential mixed component.

Epitaxially grown germanium photodiodes are used to convert the optical signals at the output ports of the directional couplers to electrical signals. Fig. 5(a) shows the structure of the photodiode, which includes a 500 nm thick germanium layer on top of a tapered waveguide to absorb the 1,550 nm light. The germanium layer in each diode, 4 μm × 16 μm in size, is the cathode node that is connected to a positive voltage externally, in order to reverse bias the diode. The anode is formed by doped regions on the sides that are connected to ground via electrical contacts. This photodiodes have a responsivity of 0.4 A/W. Since the output optical signals of the directional
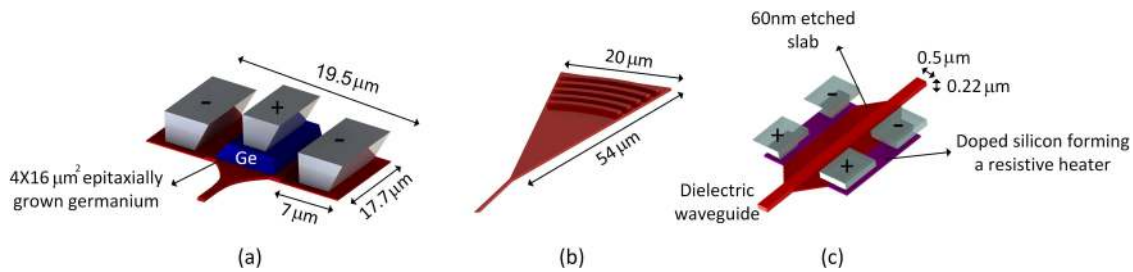
Fig. 5. (a) Germanium photodiode. (b) Focusing grating coupler. (c) Thermal phase shifter.

couplers are in the differential form, a balanced photodiode architecture [29] is used to extract the envelope of these signals, as shown in Fig. 3. The output current at the middle node of the balance structure is proportional to the differential beat tones of the optical signals.

The reference light is provided to the chip via an optical fiber through a focusing grating coupler, Fig. 5(b). The reference light is then split through a 5-level chain of splitters to thirty-two paths. As explained above, the phase shifts required for the phased array elements are applied to the reference path instead of the received signal path, which prevents the attenuation in the weak incident light path and increases the system sensitivity. Thirty-two thermal phase shifters apply the proper phase shifts to the reference signals. Each thermal phase shifter, Fig. 5(c), consists of a 500 μm long rib waveguide that carries the optical signal. The rib waveguide is connected to two ridge waveguides at the input and the output via slab tapers that convert the mode between the waveguides. There are doped regions on the sides with metal contacts that form two 940 Ω electrical resistors in parallel. These doped regions are 1 μm wide and 1.2 μm away from the center of the waveguide to avoid optical loss. The resistors heat up when an electrical current passes through them. The temperature change of the waveguide changes the refractive index of silicon waveguide, and thus the optical path length of the phase shifter. As a result, the phase of the optical signal at the output of the phase shifter can be adjusted by controlling the voltage applied to the resistors.

Both the amplitude and phase of the received signals are maintained in their associated photo-diode output current, (equation (8)). Moreover, the phase shift applied to the reference path also appears in the phase of these currents. Therefore, to achieve the desired phased array output signal, all these currents should be summed, (equation (5)). Connecting the output nodes of all the balanced photodiodes sums their currents and forms the summing point of the phased array. The resulting electrical current signal is routed to a pad on the chip so that it could be read by the off-chip electronic circuitry.

The OPA receiver is fabricated on a silicon on insulator (SOI) process with a bulk oxide thickness of 2 μm. The height of the dielectric waveguides on the chip is 220 nm, and two etch levels of 60 nm and 90 nm are used for designing grating couplers and modulators. There is also germanium photodiode in the process that makes efficient optical-electrical conversion possible. Fig. 6 shows the fabricated chip.

4. Measurement Setup

The optical schematic of the setup is shown in Fig. 7. It includes a 1,550 nm laser, the only light source in the system. The output light of the laser is split into two paths for reference and illumination. After passing through two polarization controllers, signals are input into two single side band (SSB) modulators. Polarization controllers are used to set the proper polarization for the SSB modulators. SSB modulators shift the optical frequency of illumination and reference light by $f_i = 1.15$ MHz and $f_r = 1.75$ MHz, respectively and yield the signals required for heterodyne mixing, (equations (6) and (7)). This results in a beat tone with the frequency of 2.9 MHz. This frequency was chosen to be high enough to avoid the 1/f noise of the electronics and DC offsets. The output of the SSB modulators pass through two other polarization controllers. A polarization maintaining optical fiber (PMF) is
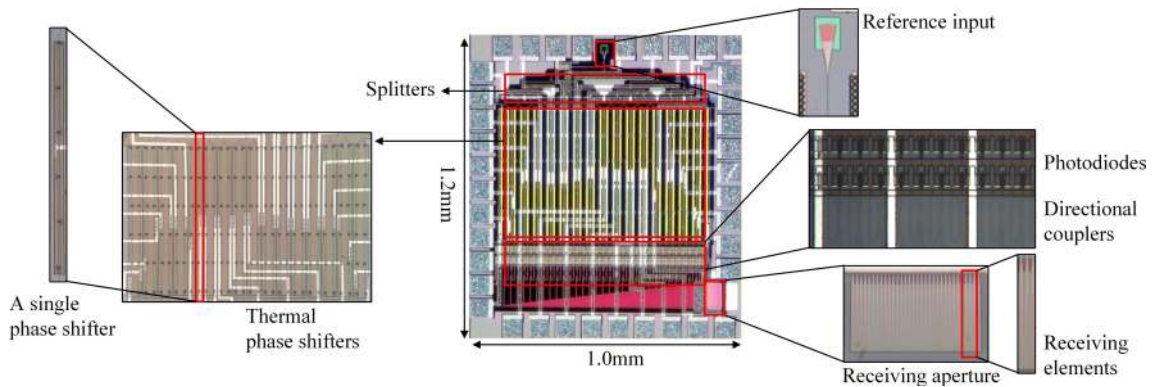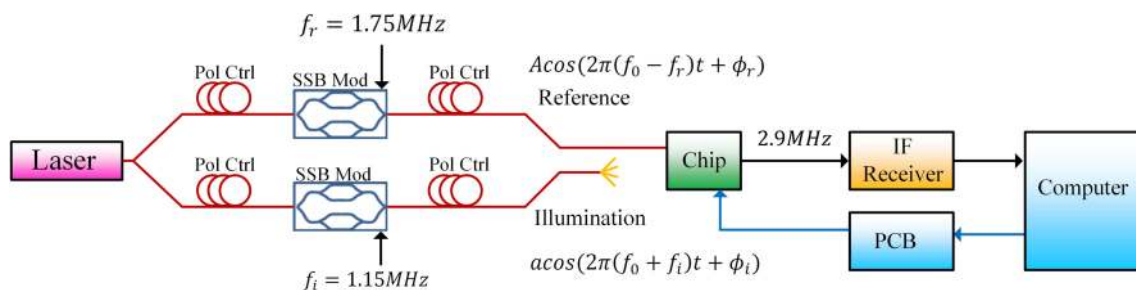
Fig. 6. Fabricated OPA receiver chip.

Fig. 7. Block diagram of the measurement setup.

used to carry the light in the reference path. The fiber tip of the reference signal is then attached with an adhesive on the on-chip focusing grating coupler, reference input, so that movements of the measurement setup do not affect the reference signal intensity.

The OPA chip is mounted on a printed circuit board (PCB) designed to control the phase shifters on the chip and process the output current of the photodiodes. Thirty-two digital-to-analog converters (DACs) followed by amplifiers are used to control the phase shifters. The output voltage range of the amplifiers is sufficient to provide 2π optical phase shift per phase shifter. A microprocessor serves as the interface between a desktop computer and the PCB. It receives commands from the computer and sends codes associated with different phase shifts to DACs. A low noise transimpedance amplifier converts the output current of the photodiodes to a voltage signal. The amplified voltage is then used for extracting and analyzing the data.

To characterize the performance of the chip, a point source is placed at different angles in front of the chip. For a given phase shifter setting, the output signal of the system for each angle yields the magnitude of the reception pattern. When a gazing beam is formed, light from most of the angles is rejected. Maximum output signal is achieved when the point source illuminates the chip from the gazing direction. Since the relative angle between the point source and the chip matters, in this setup, the point source is in a fixed location in front of the chip and the PCB is mounted on a turn table for changing the angle during the characterization process, similar to a certain antenna measurement setups.

5. Measurement and Results

Prior to performing any measurement, the chip needs to be calibrated. The calibration is needed due to the fabrication mismatches and surface roughness of the fabricated waveguides on the chip. Because of these mismatches, the delay and phase shift that light experiences traveling through the
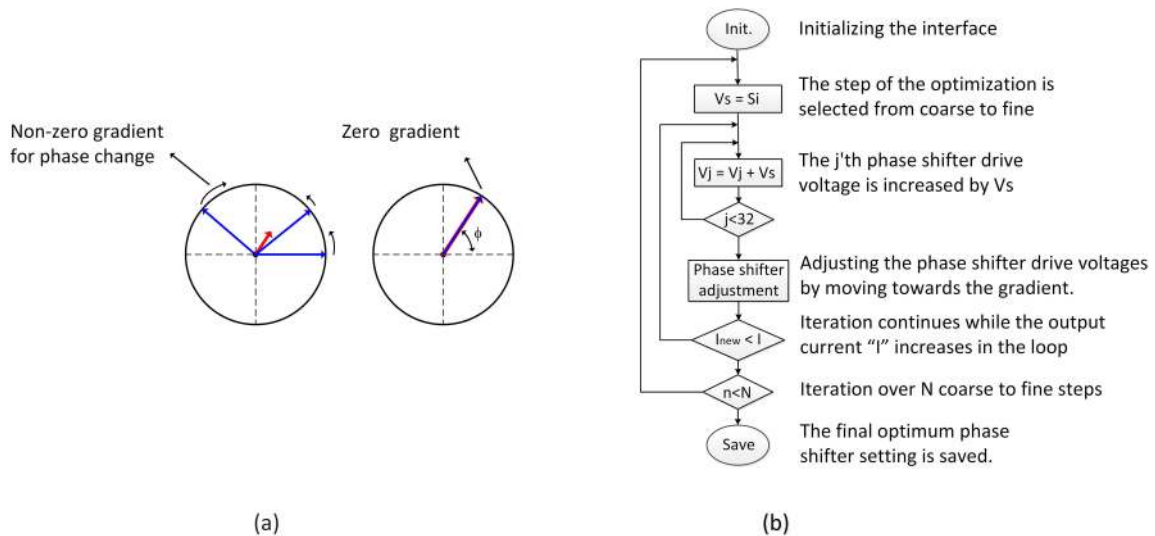
Fig. 8. (a) Demonstration of the uniqueness of the phase setting that yields the maximum output current. Blue vectors are the phasors of the signals in each of the 32 paths, and the red vector is the summation result for the blue vectors which is the output current. (b) Flowchart of the calibration algorithm used for beam forming.

waveguides deviates from an ideal rectangular waveguide [31]. Hence, when all the phase shifters are at zero phase shift, the optical signals captured by the receiving elements are not in-phase due to the different offset phase shift that light in each path experiences. To calibrate the chip, the same on chip phase shifters for beam steering can be used to cancel out the offsets, which are fixed values for each chip. Once all the phase shifters are adjusted, the received light from all the elements add up in phase and the output current amplitude is maximized. An algorithm for maximizing the output current is implemented based on the fact that if one of the phase shifters is kept unchanged as a reference (the phase shifts of the other phase shifts are measured relative to that) there is only one global maximum for the output current. Fig. 8(a) illustrates the uniqueness of the global maximum in which the output signal of each path is represented by a phasor vector. Once all the phasors are aligned in the same direction[2] (in-phase), the maximum output current is achieved. Any other configuration leads to partially destructive addition of the 32 received signals and yields a lower output current.

To maximize the output current, a gradient ascent algorithm is implemented for adjusting the phase shifters during the calibration process. In this algorithm, initially, the driving voltages of the phase shifters (determined by the DAC outputs) are changed sequentially with a coarse step and the output current changes are recorded. By collecting the effect of every phase shifter, the direction of the gradient of the output current is determined. The phase shifters are then adjusted to achieve a higher output current. This operation is performed iteratively until the maximum output is achieved. Once the output current does not improve anymore, the phase shifter step is reduced to a finner value and iteration is continued. This algorithm converges to the phase settings associated with the global maximizing.

Once the calibration phase is completed, phase shifter settings for gazing beams at all the angles are known. By applying the setting for each angle, a gazing beam in that direction is formed. To characterize the reception pattern, phase shifters are set to the associated setting for each angle. The reception patterns are extracted by rotating the turn table and measuring the amplitude of the output signal. As an example, the gazing beam for $4°$ is illustrated in Fig. 9. The 3 dB beamwidth of the gazing beam is $0.74°$. The first grating lobe happens at $30°$ which is consistent with the spacing

---

[2]This direction is the direction of the signal with the fixed phase shifter.
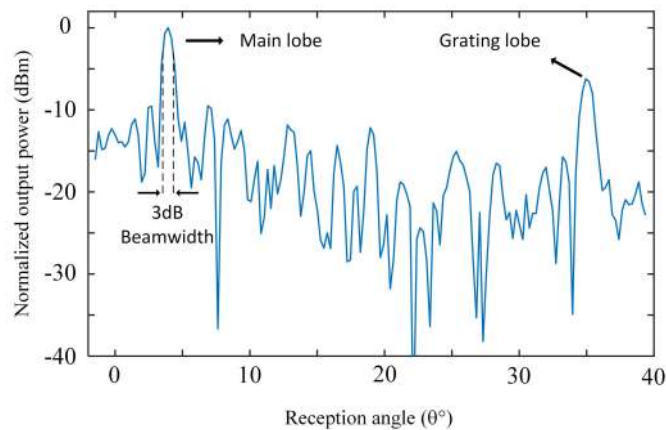
Fig. 9. Measured reception pattern of the OPA receiver for 4° after optimization.
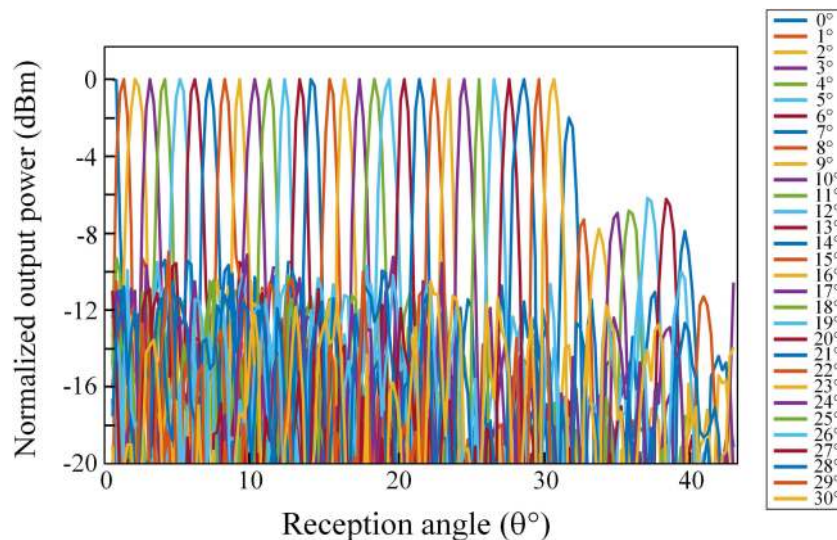

Fig. 10. Measured reception pattern of the OPA receiver for 0° − 30°.

between elements in this design. The maximum side lobe level is at least 10 dB lower than the main beam. The side lobe level can be further reduced by increasing the number of elements or adding amplitude control for the received signal at each element to improve the image quality.

Fig. 10 shows the measured patterns for different angles from 0° to 30°. The phase shifter setting for each of these patterns is loaded to the DACs through the microprocessor that is controlled with the desktop computer. If the measurement of the reception pattern is desired, turn table is used to change the relative angle between the chip and illumination source; otherwise, there is no need for the turn table. By loading each setting while the turn table is not in operation anymore, light coming from a certain direction is collected. An image is formed by combining the information collected from all the angles.

To demonstrate the imaging capability of the OPA receiver, a barcode shape object is made from a copper sheet. A piece of diffusive paper is attached to the copper piece to scatter the light illuminating it. The dimension of the object is 2 cm and it is placed at a distance of 4 cm in front of the chip to cover the 30° field-of-view. By scanning the reception angle the image of the barcode is captured. The schematic of the object, the physical object, and the captured image after applying
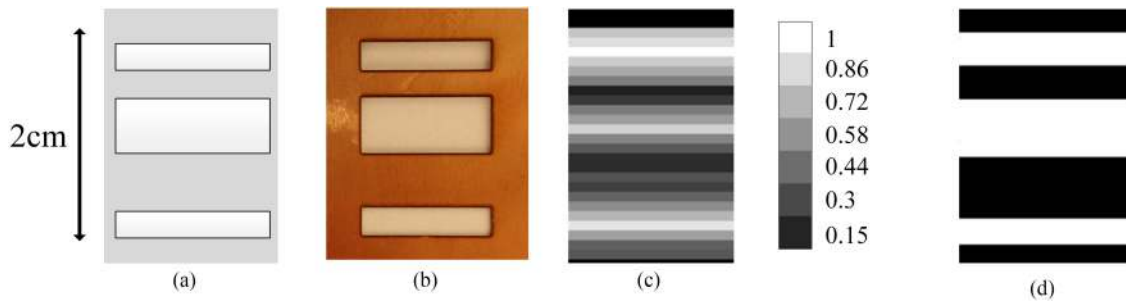
Fig. 11. (a) Barcode design. (b) Fabricated barcode from the copper sheet. (c)–(d) Captured image of the barcode in gray-scale and B&W with the OPA camera.

deterministic correction for geometrical misalignments in gray scale and black and white is shown in Fig. 11. The angle with the strongest captured signal is colored white. Black represents a signal at least 8 dB weaker and the range in between is colored in gray scale. For the black and white image of Fig. 11(d), −4 dB is chosen as the threshold in the middle of the range.

6. Conclusion

In this paper, the first heterodyne optical phased array receiver with an aperture of thirty-two receiving elements is presented. The presented heterodyne architecture with phase shifting on the reference path solves the stray light problem and significantly improves the sensitivity of the system in the presence of noise and results in a practical OPA receiver implementation. This OPA receiver can form an electronically steerable gazing beam at different angles. It can selectively collect light from a desired angle and reject others. This feature is used to realize a lens-free camera. As a lens-free camera, the OPA receiver collects light coming from different directions by steering the gazing beam and scanning the field-of-view. Having the intensity of the light impinging from all the directions, an image of the scene in front of the chip is formed. Imaging capability of the chip is demonstrated by imaging a simple barcode pattern as a proof of concept. Narrower beamwidth and higher resolution OPA cameras can be made by increasing the number of receiving element.

Acknowledgment

References

[1] G. T. Reed, G. Mashanovich, F. Y. Gardes, D. J. Thomson, "Silicon optical modulators," *Nature Photon.*, vol. 4, pp. 518–526, 2010.
[2] D. J. Thomson *et al.*, "50-Gb/s Silicon optical modulator," *IEEE Photon. Technol. Lett.*, vol. 24, no. 4, pp. 234–236, Feb. 2012.
[3] E. H. W. Chan, C. Huang, and C. B. Albert, "Optical single sideband modulator without second-order sidebands," *IEEE Photon. J.*, vol. 10, no. 3, Jun. 2018, Art. no. 7202310.
[4] L. He *et al.*, "Ultrathin silicon-on-Insulator grating couplers," *IEEE Photon. Technol. Lett.*, vol. 24, no. 24, pp. 2247–2249, Dec. 2012.
[5] M. Asaduzzaman, M. Bakaul, S. Skafidas, and M. R. H. Khandokar, "Compact silicon photonic grating coupler with dual-taper partial overlay spot-size converter," *IEEE Photon. J.*, vol. 9, no. 2, pp. 1–7, Apr. 2017, Art no. 4900107.
[6] N. Li *et al.*, "Monolithically integrated erbium-doped tunable laser on a CMOS-compatible silicon photonics platform," *Opt. Exp.*, vol. 26, pp. 16200–16211, 2018.
[7] S. Liu *et al.*, "Size scaling of photonic crystal surface emitting lasers on silicon substrates," *IEEE Photon. J.*, vol. 10, no. 3, Jun. 2018, Art. no. 4500506.
[8] J. Wang and S. Lee, "Ge-photodetectors for Si-based optoelectronic integration," *J. Sensors*, vol. 11, no. 1, pp. 696–718, 2011.

[9] C. Li, C. Xue, Z. Liu, B. Cheng, C. Li, and Q. Wang, "High-bandwidth and high-responsivity top-illuminated germanium photodiodes for optical interconnection," *IEEE Trans. Electron Devices*, vol. 60, no. 3, pp. 1183–1187, Mar. 2013.

[10] M. J. R. Heck *et al.*, "Hybrid silicon photonic integrated circuit technology," *IEEE J. Sel. Topics Quantum Electron.*, vol. 19, no. 4, Jul./Aug. 2013, Art. no. 6100117.

[11] Y. Li, Y. Zhang, L. Zhang, and A. W. Poon, "Silicon and hybrid silicon photonic devices for intra-datacenter applications: state of the art and perspectives [Invited]," *Photon. Res.*, vol. 3, no. 5, pp. B10–B27, 2015.

[12] G. Denoyer, A. Chen, B. Park, Y. Zhou, A. Santipo, and R. Russo, "Hybrid silicon photonic circuits and transceiver for 56 Gb/s NRZ 2.2 km transmission over single mode fiber," in *Proc. Eur. Conf. Opt. Commun.*, Cannes, France, 2014, pp. 1–3.

[13] B. Abiri, F. Aflatouni, A. Rekhi, and A. Hajimiri, "Electronic two-dimensional beam steering for integrated optical phased arrays," in *Proc. Opt. Fiber Commun. Conf.*, 2014, Paper M2K.7.

[14] S. Chung, H. Abediasl, and H. Hashemi, "A 1024-element scalable optical phased array in 0.18 μm SOI CMOS," in *Proc. IEEE Int. Solid-State Circuits Conf.*, San Francisco, CA, USA, 2017, pp. 262–263.

[15] C. V. Poulton *et al.*, "Large-scale silicon nitride nanophotonic phased arrays at infrared and visible wavelengths," *Opt. Lett.*, vol. 42, pp. 21–24, 2017.

[16] D. Hutchison *et al.*, "High-resolution aliasing-free optical beam steering," *Optica*, vol. 3, pp. 887–890, 2016.

[17] J. Hulme *et al.*, "Fully integrated hybrid silicon free-space beam steering source with 32-channel phased array," *Proc. SPIE*, vol. 8989, 2014, Art. no. 898907.

[18] B. Ortega, J. Mora, and R. Chulia, "Optical beamformer for 2-D phased array antenna with subarray partitioning capability," *IEEE Photon. J.*, vol. 8, no. 3, Jun. 2016, Art. no. 6600509.

[19] R. Fatemi, A. Khachaturian, and A. Hajimiri, "Scalable optical phased array with sparse 2D aperture," in *Proc. Conf. Lasers Electro Opt.*, 2018, Paper STu4B.6.

[20] R. C. Hansen, *Phased Array Antennas.* New York, NY, USA: Wiley, 2009.

[21] J. Hasch, E. Topak, R. Schnabel, T. Zwick, R. Weigel, and C. Waldschmidt, "Millimeter-wave technology for automotive radar sensors in the 77 GHz frequency band," *IEEE Trans. Microw. Theory Tech.*, vol. 60, no. 3, pp. 845–860, Mar. 2012.

[22] A. Hajimiri, A. Komijani, A. Natarajan, R. Chunara, X. Guan, and H. Hashemi, "Phased array systems in silicon," *IEEE Commun. Mag.*, vol. 42, no. 8, pp. 122–130, Aug. 2004.

[23] D. Tseng *et al.*, "Lensfree microscopy on a cellphone," *Lab Chip*, vol. 10, pp. 1787–1792, 2010.

[24] T. Komljenovic, R. Helkey, L. Coldren, and J. E. Bowers, "Sparse aperiodic arrays for optical beam forming and LIDAR," *Opt. Exp.*, vol. 25, pp. 2511–2528, 2017.

[25] C. T. Phare, M. C. Shin, J. Sharma, S. Ahasan, H. Krishnaswamy, and M. Lipson, "Silicon optical phased array with grating lobe-free beam formation over 180 degree field of view," in *Proc. Conf. Lasers Electro Opt.*, 2018, Paper SM3I.2.

[26] H. Abedias and H. Hashemi, "Monolithic optical phased-array transceiver in a standard SOI CMOS process," *Opt. Exp.*, vol. 23, pp. 6509–6519, 2015.

[27] R. Fatemi, B. Abiri, and A. Hajimiri, "A one-dimensional heterodyne lens-Free OPA camera," in *Proc. Conf. Lasers Electro Opt.*, 2016, Paper STu3G.3.

[28] R. Fatemi, B. Abiri, and A. Hajimiri, "An 8 $\times$ 8 heterodyne lens-less OPA camera," in *Proc. Conf. Lasers Electro Opt.*, 2017, Paper JW2A.9.

[29] K. Ho, *Phase-Modulated Optical Communication Systems.* New York, NY, USA: Springer, 2005, ch. 3.

[30] M. Raval, C. Poulton, and M. Watts, "Unidirectional waveguide grating antennas with uniform emission for optical phased arrays," *Opt. Lett.*, vol. 42, pp. 2563–2566, 2017.

[31] Y. Yang *et al.*, "Phase coherence length in silicon photonic platform," *Opt. Exp.*, vol. 23, pp. 16890–16902, 2015.